IAC-25-C1-IP-48-x103096

Low-Cost rendezvous and phasing with the Lunar Gateway leveraging quasi-periodic tori

Matteo Santacesaria [a]*, **Nathaniel Phillip Sailor** [b]*, **Andrea Capannolo** [c]*, **Andrea De Vittori** [d]*

[a] *M.Sc. Space Engineering, Politecnico di Milano, Italy,* E-mail: matteo.santacesaria@mail.polimi.it

[b] *M.Sc. Student, School of Aeronautics and Astronautics, Purdue University, West Lafayette, IN, United States.* E-mail: nsailor@purdue.edu

[c] *Assistant Professor, School of Aeronautics and Astronautics, Purdue University, West Lafayette, IN, United States.* E-mail: acapa@purdue.edu

[d] *Postdoctoral Researcher, School of Aeronautics and Astronautics, Purdue University, West Lafayette, IN, United States.* E-mail: adevitto@purdue.edu

* Corresponding author

Abstract

In recent years, the cislunar environment has emerged as a vital base for space research and a stepping stone to destinations like Mars. The development of the Lunar Gateway is a result of this trend. In fact, it will support experiments, serve as a refueling hub, and facilitate the construction of a human outpost on the Moon. For these reasons, cost-effective transport to and from the station's orbit will be pivotal in maximizing its potential. Additionally, constraints on launch dates are currently a driving factor during the mission design, leading to suboptimal solutions during spacecraft development. The current state of the art exploits periodic orbits to identify efficient Earth-to-Moon transfer trajectories. This work leverages the manifold theory to extend that concept to quasi-periodic orbits in the Three-Body Problem and exploits their properties to retrieve a more efficient path to the station. In fact, manifolds are natural trajectories that do not require active propellant consumption from the spacecraft. The objective is to optimize the approach to the Lunar Gateway by balancing fuel consumption and operational flexibility. This solution reduces dependency on fixed launch dates and expands the range of feasible mission profiles while minimizing overall transfer propellant costs. Numerical methods are used to generate quasi-periodic tori around the initial and target orbits, and interpolating functions are retrieved for each torus. These analytical curves can be later exploited to identify the intersections between tori and produce feasible transfer trajectories to the Lunar Gateway, reducing propellant needs. These transfers also serve as starting conditions for an optimization algorithm that models the finite-burn maneuvers. The outcome of this study is the identification of optimized trajectories that outperform current baseline solutions, offering advantages in terms of reduced fuel consumption and enhanced scheduling flexibility. This investigation contributes to the sustainability and cost-effectiveness of lunar exploration, paving the way for human presence on the Moon and future missions to Mars and beyond.

1. Introduction

From The United States Code, title 42 USC 18302 [1]: The term "cis-lunar space" means the region of space from the Earth out to and including the region around the surface of the Moon.

During the Cold War, the United States and the Soviet Union competed in a political "space race" to land humans on the Moon. Once that goal was achieved, since there was no plan to establish a permanent lunar outpost or use the Moon as a staging ground for other missions, interest and funding for crewed lunar flights waned after the Cold War ended. In recent years, however, cislunar space has regained prominence as a venue for science, and strategic operations. Beyond the capabilities of low-Earth and geosynchronous orbits, it offers deep-space observation, long-duration experimentation, and staging for interplanetary missions [2]. Near-lunar space in particular provides an ideal testbed for advanced transportation systems destined for Mars, near-Earth asteroids, and beyond.

Economically and technologically, building infrastructure in cislunar space could enable space manufacturing, tourism, and improve the sustainability for the exploration of the solar system. Proposed elements include propellant depots, in-orbit servicing platforms, and facilities that harvest lunar ice for in-situ resource utilization [3]. Together, these would support refueling stations, spacecraft assembly hubs, and communication relays. Cislunar operations also open unique scientific opportunities, such as studies of long-term habitation, radiation effects, and novel propulsion in a deep space environment, which are impossible within Earth's magnetosphere. Such research will underpin future human and robotic missions beyond the Moon.

Robotic spacecraft have already mapped much of this domain: NASA's GRAIL mission measured the Moon's gravity via long-distance transfers, and the ARTEMIS probes explored the Earth–Moon Lagrange regions up to 1.5 million kilometers away [3]. More recently, the CAPSTONE cubesat demonstrated autonomous navigation in a Near-Rectilinear Halo Orbit (NRHO), and the forthcoming Cislunar Highway Patrol System will provide persistent space-domain awareness in lunar vicinity [3]. To prepare for human return, the Lunar Gateway, a crewed station in NRHO, will offer habitation, power, propulsion, docking ports, and an airlock. Drawing on the experience gained with the International Space Station, it will serve as a reusable node for research, technology demonstration, and crew transfers to the lunar surface and beyond [3].

Operating in cislunar space presents significant challenges: three-body dynamics demand specialized trajectory models and frequent state updates; many Lagrange-point and halo orbits are inherently unstable, driving high station-keeping costs [3]; and the vast distances complicate sensing and tracking. Before a true cislunar economy can flourish, it is necessary to establish a reliable logistics that will require multipurpose infrastructure, such as fuel depots, power distribution, standardized interfaces, and on-orbit servicing. On top of that, lunar resource extraction must overcome the problems related to extreme thermal and illumination conditions [2].

As technology advances, the cislunar region will become the foundation for interplanetary travel, supporting scientific breakthroughs and commercial ventures that shape the next era of exploration. The investment and collaboration of NASA, ESA, JAXA, and CSA in designing and building the Gateway underscore its central role in this emerging ecosystem. During its construction and operation, efficient, reliable, and flexible access to the Gateway will be crucial to sustain the dozens of missions that will shuttle crews and cargo back and forth from Earth.

By this means, lately, new strategies to exploit the n-body dynamics have been explored. Henry and Scheeres [4] introduce a whisker-intersection approach using the stable and unstable manifolds of quasi-periodic tori to generate "natural" transfers between QPOs (Quasi periodic Orbits). Jain and Howell [5] present two complementary frameworks: locally fuel-optimal impulsive maneuvers and two-maneuver interior-type or three-maneuver exterior-type transfers that link Near-Rectilinear Halo Orbits (NRHO) and Distant Retrograde Orbits (DRO) via QPO manifolds. Duering [6] exploits the hyperbolic invariant manifolds of QPOs and periodic orbits to perform transfers among tori in the Earth-Moon system. McCarthy and Howell [7] leverage QPO families and their associated manifolds for cislunar trajectory design and eclipse avoidance. Finally, Jain [8] outlines a systematic methodology that uses the five-dimensional manifolds of QPO families to construct interior and exterior transfers between periodic orbits.

Although these strategies can yield low-cost transfers, they require an optimization process that is highly sensitive to the initial conditions, both in terms of solution quality and computational cost. In fact, all these strategies use disconnected orbits as initial guesses that do not represent actual trajectories. This makes the optimization algorithm converge slower and possibly not to the optimal solution. This work proposes a method to identify feasible transfer orbits and use them as informed initial guesses to guide the optimization process. By narrowing the search space and focusing on promising regions, the approach promises to accelerate convergence and avoid providing solutions with prohibitively high fuel consumption during the design of the finite-burn maneuver.

The quasi-periodic tori are generated using the Gomez, Mondelo, Olikara, and Scheeres (GMOS) scheme, and a set of orbits for each torus is propagated to retrieve a grid on which the torus itself can be interpolated via bi-cubic splines. Once analytical curves are recovered for the full state vector, the interpolation points between these two curves are retrieved. In the end, the corresponding impulsive Δv to maneuver to the target torus is computed. These solutions are used as initial conditions for the finite-burn optimization algorithm, searching in the surroundings of the minimum Δv retrieved on the intersection curve. This process, once a starting position and a target object orbiting the Moon are fixed, also allows for phasing, exploiting quasi-periodic trajectories as parking orbits. Through this approach, a satellite is able to rendezvous with the desired object with no need for additional active phasing maneuvers.

In the following chapters the method proposed in the paper is carefully described and the results are presented. The paper starts with a brief recap on the background knowledge and the CR3BP. Later, the retrieval of the initial conditions for the orbits under analysis, and how those are used to generate an interpolating grid are described. After that, the interpolation process is presented, and the results obtained with different grids are compared. In the end, the optimal transfers are computed and the results are summed up and discussed.

2. Background

The work is developed in the framework of the Circular Restricted Three-Body Problem (CR3BP), in this model, the two primary bodies (Earth and Moon) are orbiting on circular orbits around the center of mass, and their motion is not influenced by the position of the third body (the spacecraft).

Following the work of Ferrari [9], the acceleration of the third body in the rotating reference frame is retrieved. Equation 1 and Equation 2 show the resulting formulas.

$$\begin{cases} \ddot{x}_3 - 2\dot{y}_3 &= \dfrac{\partial U}{\partial x_3} \\ \ddot{y}_3 + 2\dot{x}_3 &= \dfrac{\partial U}{\partial y_3} \\ \ddot{z}_3 &= \dfrac{\partial U}{\partial z_3} \end{cases} \tag{1}$$

$$U(x_3, y_3, z_3) = \frac{1}{2}(x_3^2 + y_3^2) + \frac{1-\mu}{r_1} + \frac{\mu}{r_2} \tag{2}$$

In the CR3BP, the linearization about a libration point yields two real eigenvalues $\pm a$ (hyperbolic directions) and two imaginary eigenvalues $\pm ib$ (elliptic directions). The associated unstable (W^u) and stable (W^s) manifolds form tubes that carry trajectories away from or toward the vicinity of the libration point, while the central manifold (W^c) contains bounded, oscillatory motion (like halo and Lyapunov orbits) arising from the imaginary modes. These invariant structures enable low-cost transfers between different regions of the phase space.

A quasi-periodic torus (W^c) wraps around a parent periodic orbit, tracing out a two-dimensional a closed surface around the periodic orbit in phase space. Each torus is characterized by its fundamental period T and twist angle per revolution ρ. By introducing angle coordinates (θ_1, θ_2) with frequencies (ω_1, ω_2), it is possible to parameterize the toroidal surface and locate any point on it at time t:

$$\begin{cases} \theta_1 = \theta_{1i} + \omega_1 t \\ \theta_2 = \theta_{2i} + \omega_2 t \end{cases} \tag{3}$$

The angles θ_1 and θ_2 have the properties:

$$\begin{cases} \theta_1(t) = \theta_1(t+T) - 2\pi \\ \theta_2(t) = \theta_2(t+T) - \rho \end{cases} \tag{4}$$

where T is the period associated to the first angle (θ_1) and ρ is the twist angle, corresponding to the drift of θ_2 after 1 revolution of period T. Figure 1 helps to visualize the parameterization angles.

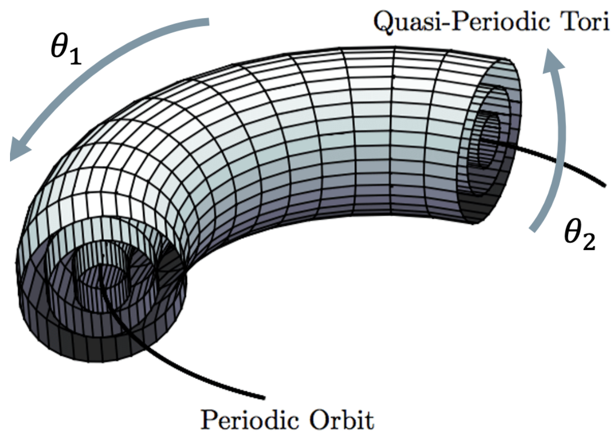

Fig. 1: Parametrization angles visualization. [10]

3. Grid generation and tori interpolation

In the process described in the introduction, the first step is to identify a periodic orbit in the Earth-Moon Three-Body problem and retrieve a set of quasi-periodic orbits around it. The initial periodic orbit is a 9:2 resonant Near-Rectilinear Halo Orbit (NRHO) [11], from this one another one from the same family has been retrieved, having a period 20% longer. The first one is, as of today, the operative orbit of the Lunar Gateway, while the second one has been selected for the study because is a suitable parking orbit for missions to the station.

The scheme reported in Figure 2 is used to retrieve periodic orbits.

Three basic tools are needed:

1. A good initial condition to start with should be available: the six-dimensional initial state should be close enough to the state of a periodic orbit.

2. Once a good initial condition is provided, the second step consists in the correction of this initial guess, imposing constraints on the initial state, in order to retrieve the periodic orbit.

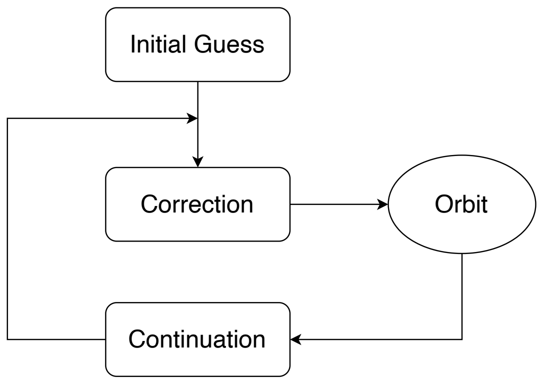

Fig. 2: Orbit computation algorithm.

3. Finally, once a periodic orbit is given, to compute the entire family, a continuation method is implemented.

A similar process is implemented for the computation of quasi-periodic orbits, exploiting the GMOS (Gómez, Mondelo, Olikara and Scheeres algorithm [12]). With these tools implemented and put together in an algorithm, it is possible to compute the initial conditions for the desired orbits and generate families of tori in its neighborhood.

Using the GMOS scheme, a set of initial conditions is computed for different branches of a quasi-periodic orbit belonging to a family of tori. After selecting a specific torus, these initial states are propagated to generate the corresponding set of orbits, which are then used to construct the interpolating grid for the subsequent analysis. In Table 1 are highlighted the initial conditions for the periodic orbit used to generate the torus, all the values have been non-dimensionalized considering for the Earth-Moon system: $L^* = 384400\ km$, $t^* = 375196\ s$ and $\mu = 0.012150$.

Table 1: Initial conditions for the 9:2 periodic NRHO and the one with 120% the period of the Lunar Gateway.

States	Gateway [nd]	120% Period [nd]
x_0	1.02134	1.043539
y_0	0	$4.878772 \cdot 10^{-3}$
z_0	-0.18162	-0.193594
V_{x0}	0	$5.816054 \cdot 10^{-3}$
V_{y0}	-0.10176	-0.145463
V_{z0}	$9.76561 \cdot 10^{-7}$	$-1.480161 \cdot 10^{-2}$
Period	1.50206	1.802472

After the orbits are propagated using the equations highlighted in the background chapter for the Circular Restricted Three-Body Problem (CR3BP), a grid of discretized states is available.

However, to achieve an accurate interpolation some post-processing is required: three different techniques to distribute the nodes have been considered, equally spaced in time, space traveled, or velocity variation. In this way, it is possible to analyze the results for a grid with the nodes concentered at the apolune, perilune, or equally spaced. In addition to that, since the quasi-periodic orbits are wrapping around the periodic orbits, a counter-rotation of the nodes was necessary to ensure a regular grid.

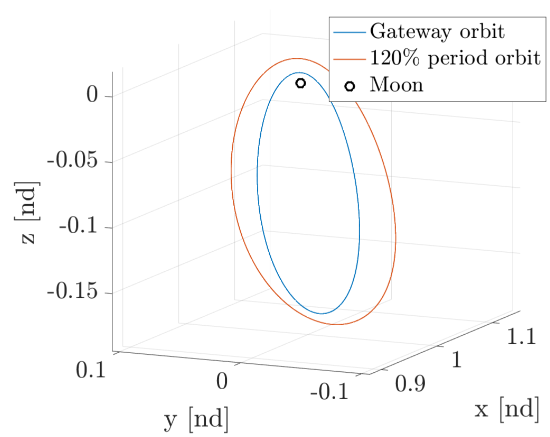

Fig. 3: Propagated orbits in the non-dimensional rotating reference frame.

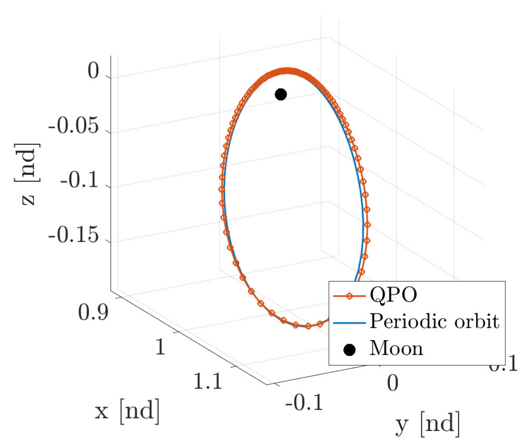

Fig. 4: Discrete grid points in the non-dimensional rotating reference frame.

Although this process is simple from a logical point of view, its coding implementation requires few steps:

1. A vector of times is created to have the points equally spaced in time, space, or velocity variation.
2. For all the time values retrieved, the initial θ_2 is computed as $\theta_{2i} = \theta_{2\ node} - \omega_2 t_{point}$.
3. An spline interpolation of the initial stroboscopic map is required to be able to start propagating an orbit for any needed value of θ_{2i}, the resulting interpolated map is highlighted in Figure 5.
4. The initial state is propagated for the desired amount of time and the point is added to the grid.

This ensures that for $t = t_{point}$, $\theta_2 = \theta_{2\ node}$, therefore all the nodes of the same branch have the same θ_2 value.

Figure 3 shows the two periodic orbits selected to for the analysis and Figure 4 the velocity based grid after the post processing described above. The torus generated and the stroboscopic map interpolated are highlighted in Figure 5.

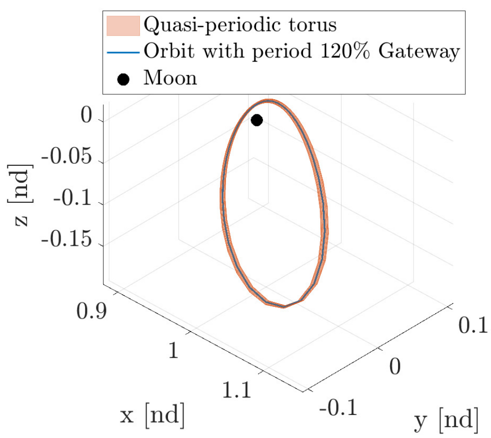

Fig. 5: Torus computed around the periodic orbit in the non-dimensional rotating reference frame.

Once all the grids are generated, the interpolation has been performed using `griddedInterpolant` from Matlab and setting it to use a bi-cubic spline. All grids use 100 nodes for the first frequency (θ_1) and 30 nodes for the second (θ_2), generating a 30 by 100 matrix for each element of the state vector to feed into the interpolation.

3.1 Interpolation results

The results in Figures 7 to 12 highlight that the grid based on velocity variation performs slightly better than the one based on the distance traveled, while the one based

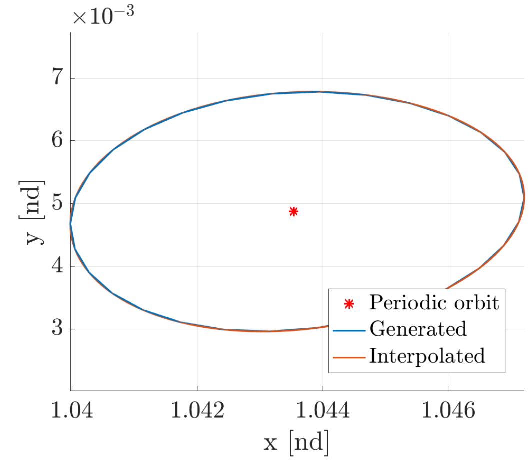

Fig. 6: Interpolated stroboscopic map at $t = t_0$ in the non-dimensional rotating reference frame.

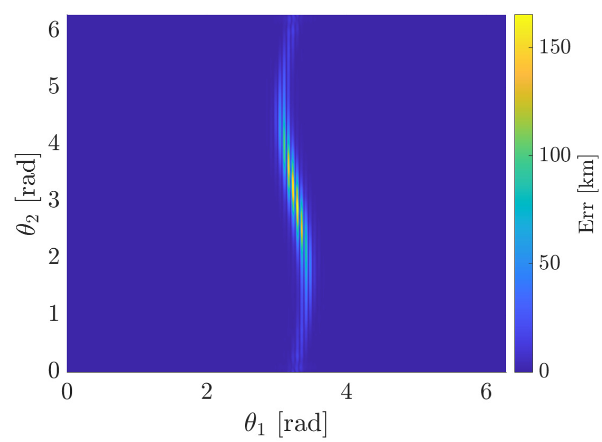

Fig. 7: Error in position interpolating with a grid equally spaced in time, torus with 120% the period of the Gateway.

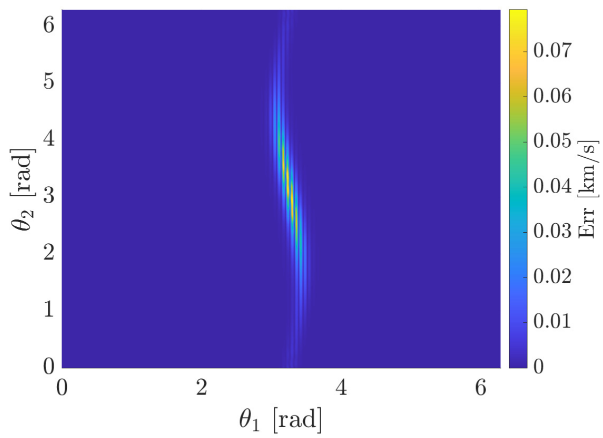

Fig. 8: Error in velocity interpolating with a grid equally spaced in time, torus with 120% the period of the Gateway.

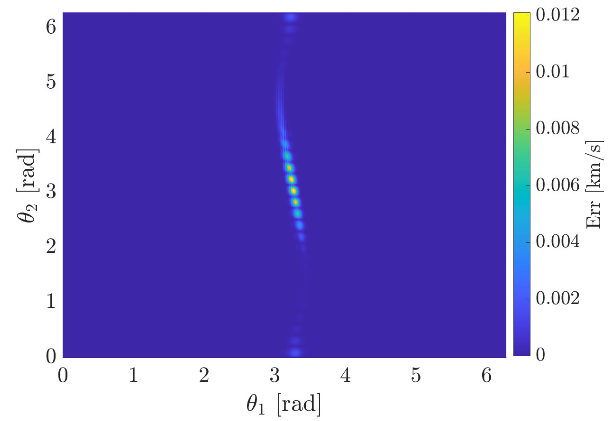

Fig. 10: Error in velocity interpolating with a grid equally spaced in distance traveled, torus with 120% the period of the Gateway.

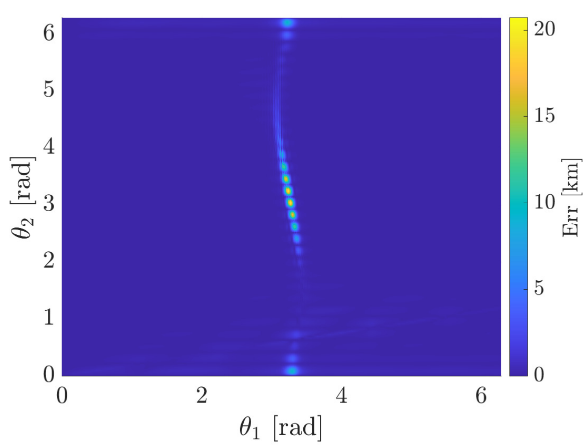

Fig. 9: Error in position interpolating with a grid equally spaced in distance traveled, torus with 120% the period of the Gateway.

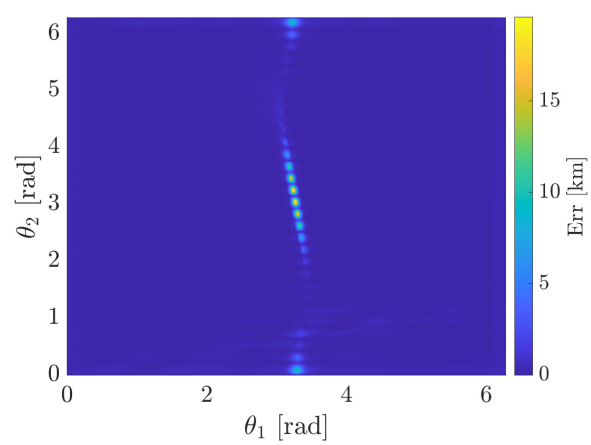

Fig. 11: Error in position interpolating with a grid equally spaced in velocity variation, torus with 120% the period of the Gateway.

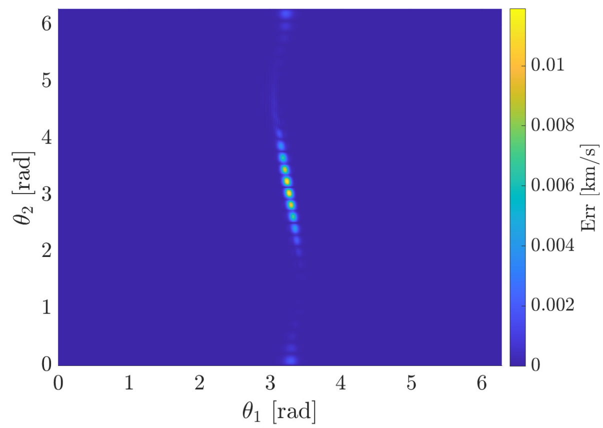

Fig. 12: Error in velocity interpolating with a grid equally spaced in velocity variation, torus with 120% the period of the Gateway.

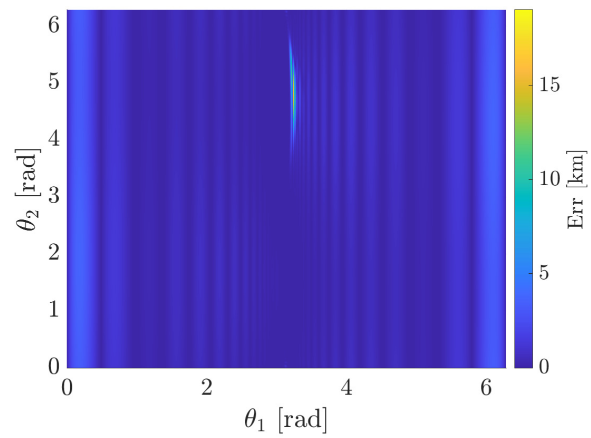

Fig. 13: Error in position interpolating with a grid equally spaced in velocity variation, torus about the orbit of the Gateway.

on time gives less accurate results. The time grid is not capable of representing the torus with good accuracy around the perilune. The other two grids are working significantly better but the grid based on the distance is less accurate in representing the torus around the perilune. These results are compliant with what was expected since the velocity-based grid has a higher concentration of nodes at the perilune, where the derivative of the state vector is larger. For this reason, the grid selected for the interpolation is the velocity-equispaced one. Given the small distance between the results with the space and velocity based grids, it has been decided not to pursue grids pushing even more nodes to the perilune, such as building a grid based on acceleration.

Figures 11 and 12 show that the interpolating errors are within acceptable ranges for the torus with $\sim$ 120% the period of the Gateway. In fact, given the long distances in place in astrodynamics, and the fact that the interpolation has the only goal of quickly retrieving initial conditions that will be better refined during the design of the maneuver and optimization of the transfer, an error in the order of 10 km for the distances and of the 10 m/s for the velocities is considered acceptable. The same analysis is carried out for the torus derived from the Gateway's orbit, and after refining the grid by increasing the number of nodes in the stroboscopic map from 30 to 100, acceptable errors are found again. (Figures 13 and 14)

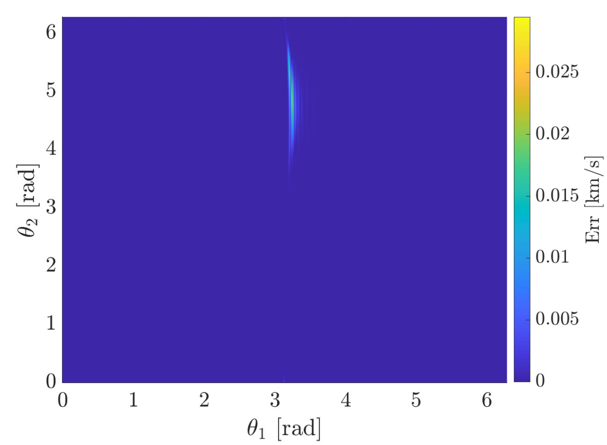

Fig. 14: Error in velocity interpolating with a grid equally spaced in velocity variation, torus about the orbit of the Gateway.

4. Tori intersection points retrieval

After computing the interpolating function for two tori around two periodic orbits, the intersection points are computed.

The first point is retrieved through an `fsolve` optimization aimed to make the position of the two tori match. The initial conditions for this process are retrieved through a grid search on the points of the grids used to interpolate the tori. Equation 5 shows the match conditions fed into `fsolve`.

$$\mathbf{F}(\mathbf{r_1}, \mathbf{r_2}) = \begin{bmatrix} r_{x\ torus1} - r_{x\ torus2} \\ r_{y\ torus1} - r_{y\ torus2} \\ r_{z\ torus1} - r_{z\ torus2} \end{bmatrix} = \mathbf{0} \qquad (5)$$

The intersection curve between two implicitly defined tori is computed using a predictor-corrector-continuation method based on pseudo-arclength parametrization. Continuation along the solution branch is achieved by first determining the tangent direction as the null space of the Jacobian matrix, using the Jacobian computed numerically during the optimization process.

$$null(\mathbf{J}(\mathbf{X_{prev}})) \cdot (\mathbf{X} - \mathbf{X_{prev}}) - \delta s = 0 \qquad (6)$$

where δs is the pseudo-arclength step size and $null(\mathbf{J}(\mathbf{X_{prev}}))$ is the tangent vector to the solution curve at the previous point. This estimate is then refined through a corrector step by solving an augmented system comprising both Equation 5 and the pseudo-arclength constraint reported in Equation 6. The inclusion of this constraint ensures the robustness of the continuation procedure across folds or turning points along the intersection curve.

Figure 15 shows the intersection points and the resulting intersection curves, while Figure 16 shows the Δv necessary to complete an impulsive maneuver and move to the second torus.

From the results, it can be seen that the intersection curve is retrieved as intended, and the Δv requirement changes depending on the maneuvering position. Looking at the Δv profile is possible to see a minimum: that region is a well-suited guess for an optimization with the finite-burn model, leading to a more realistic transfer design that withstands the maximum thrust level available on the spacecraft.

As a last step, the transfer opportunities are retrieved setting the initial position of the spacecraft on the phasing torus (Torus 1) as $\theta_1 = \theta_2 = 0$ at the initial time. In Figure 17 the transfer opportunities are highlighted, being the intersection between the propagated position of the spacecraft and the intersection curves retrieved before.

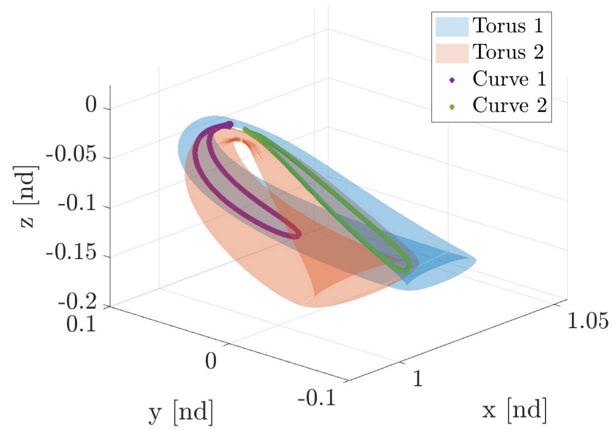

Fig. 15: Intersection curves between the tori in the non-dimensional rotating reference frame.

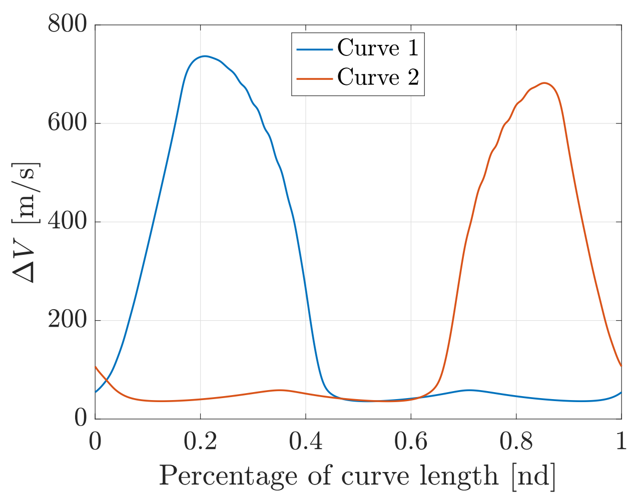

Fig. 16: Δv along the intersection curve.

Figure 18 highlights the transfer opportunities with respect to the time to better visualize the frequency of encounter.

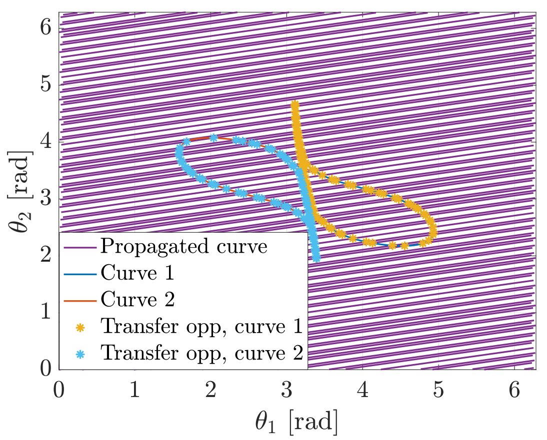

Fig. 17: Quasi-periodic motion of the spacecraft (purple lines) and intersection curves.

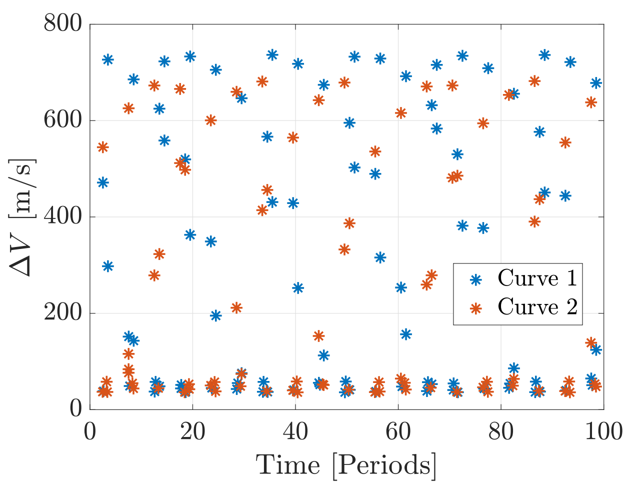

Fig. 18: Transfer opportunities over time.

A total of 170 transfer opportunities is retrieved over 100 revolutions on the phasing torus (Torus 1), 81 of them being below 100 m/s of required impulse. This mean that, on an average, there is one low-cost transfer opportunity every 9.7 days. This relatively high frequency of encounter with the targeted torus allows more flexibility during the mission design, opening the chance to a larger variety of launch date epochs.

5. Transfer design

Once all the transfer opportunities are retrieved, the design of the transfers is carried out. The simulation of the complete transfer from a Low Earth Orbit (LEO) to the Gateway is divided into three different steps, obtaining the optimal trajectory for all the legs:

1. Transfer from LEO to the torus with ∼ 120% the period of the Gateway.

2. Transfer from that torus (Torus 1) to the one around the orbit of the Gateway (Torus 2).

3. Rendezvous with the station.

This strategy is compared with another one that just targets the orbit of the Gateway starting from the same LEO used in the other strategy. The goal of this analysis is to retrieve the difference in transfer cost and flexibility of the two strategies.

The optimal trajectories are computed using a genetic algorithm (`ga`) for retrieving good initial conditions for all the variables, and a gradient-based algorithm (`fmincon`) to refine the solution and obtain the optimal transfer. The choice of including a genetic algorithm in the loop is driven by the fact that, even if the initial guess for the impulsive transfer is accurate, there are some quantities needed for the two-impulse or finite-burn transfers that are not defined in a single-impulse maneuver, therefore an accurate initial guess in not available for these variables. An example is the coasting time between the two impulses. This method allows for finding the local minimum within the boundaries provided. In Figure 19 is reported a block diagram of the optimization adopted.

In terms of workflow, the functions that simulates the trajectory are all structured as in Figure 20, minor variations between the different cases are applied to comply with the specific transfer under investigation. However, all the simulations rely on a two-maneuver strategy to complete the transfers. The simulation takes as input the initial conditions and propagates the trajectory until the starting time of the first burn (t_{1i}), the burn is performed (either impulsive or finite-burn), and the transfer trajectory is propagated until the beginning of the second burn (t_{2i}), also the second burn is performed and the final trajectory is propagated to the apolune for the evaluation of the constraints (if present) and cost function. If the maneuvers are impulsive: $t_{1i} = t_{1f}$ and $t_{2i} = t_{2f}$.

The optimization aims at minimizing the total impulse and reads:

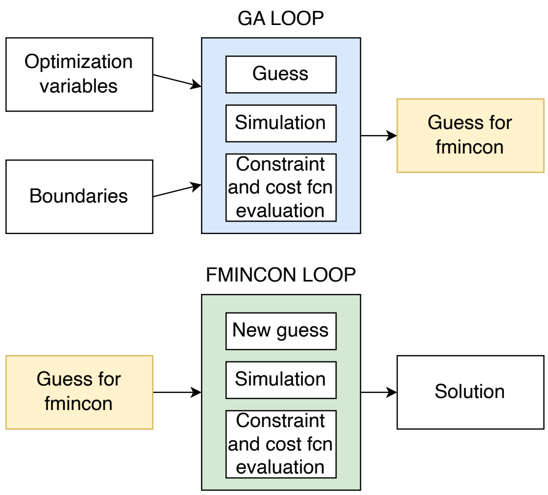

Fig. 19: Block diagram of the optimization process.

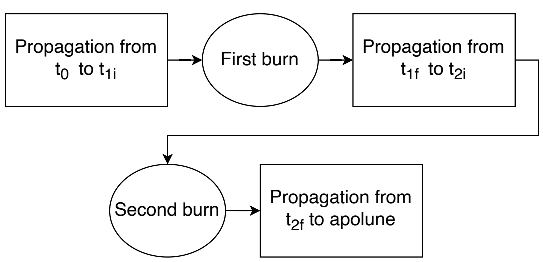

Fig. 20: Block diagram of the trajectory simulation process.

$$
\begin{aligned}
\min_{\substack{\Delta\mathbf{v}_1,\Delta\mathbf{v}_2,\\ t_1,t_2}} \quad & J(\Delta\mathbf{v}_1,\,\Delta\mathbf{v}_2) = \|\Delta\mathbf{v}_1\| + \|\Delta\mathbf{v}_2\| \\
\text{S.t.} \quad & \dot{\mathbf{X}}(t) = \mathbf{f}(\mathbf{X}(t),t) \\
& \mathbf{X}(t_0) = \mathbf{X}_0 \\
& t_0 \le t_1 < t_2 \le t_f \\
& \mathbf{X}(t_1^+) = \mathbf{X}(t_1^-) + [0,\ 0,\ 0,\ \Delta\mathbf{v}_1]^T \\
& \mathbf{X}(t_2^+) = \mathbf{X}(t_2^-) + [0,\ 0,\ 0,\ \Delta\mathbf{v}_2]^T \\
& \mathbf{X}(t_f) = \mathbf{X}_f
\end{aligned} \tag{7}
$$

with $\Delta\mathbf{v_1}$ and $\Delta\mathbf{v_2} \in \mathbb{R}^3$ being the impulses of the maneuvers, $\mathbf{X} \in \mathbb{R}^6$ the state vector, and $\mathbf{f} : \mathbb{R}^6 \to \mathbb{R}^6$ is the function containing the equations of motion of the CR3BP. t_1 and t_2 are the time instants of the first and second burn. In the optimization loops the Δv vectors are computed starting from a unit vector in the x direction and performing the rotations around y and z compliant with the σ values adopted. The mathematical expression is reported in Equation 8.

$$
\Delta\mathbf{v}_i = \mathbf{R_z}(\sigma_{iz}) \cdot \mathbf{R_y}(\sigma_{iy}) \cdot [1,0,0]^T \Delta v_i \tag{8}
$$

with $\mathbf{R_z}$ and $\mathbf{R_y}$ being rotation matrices around the z and y-axis.

5.1 Transfer between two tori

This transfer has been simulated under the assumption of impulsive transfer following Equation 7.

5.2 Rendezvous with the station

A similar approach is followed to compute the optimal transfer to rendezvous with the station. This maneuver is the last one performed before the docking phase, the aim is to get as close as possible to the station to allow the proximity operations to start and dock the spacecraft correctly. The optimization process follows the block diagram in Figure 19 to retrieve the minimum Δv required to complete the transfer. The maneuvers simulated are considered impulsive. Both the station and the spacecraft are assumed to be at the apolune at the beginning of the simulation. The state of the spacecraft is taken from the results of the transfer between the two tori, propagated to the apolune. The constraints aim at matching the orbit of the Gateway, while also ensuring the match of the phase θ_1 at the arrival of the spacecraft on the target orbit, therefore the following constraint is added to Equation 7.

$$
\theta_{1f}(t) = \theta_{1f}^{GW}(t) \tag{9}
$$

An important adjustment to make is, instead of using the initial conditions for the Gateway previously retrieved from Zimovan [11], to correct that orbit retrieving more significant digits and improving the accuracy of the target orbit, otherwise the algorithm struggles to converge.

5.3 Earth-NRHO transfer

The initial conditions are computed starting from the Keplerian elements of a LEO, this orbit is chosen because it is a typical target orbit for a launch from Cape Canaveral, Florida [13].

The fitness function receives the spacecraft state in LEO, $\mathbf{X}_{LEO}$, and the state at the target orbit's apolune, $\mathbf{X}_{target}$, then retrieves the impulses necessary to reach the target starting from the initial state. Rather than imposing explicit constraints, each iteration calls `fsolve` to determine

Table 2: LEO Keplerian elements.

Orbital elements	**Values**
a [km]	6578.1
e [nd]	0
i [deg]	28.5
ω [deg]	0
Ω [deg]	90
θ [deg]	0

the first impulse, $\Delta\mathbf{v}_1$, required to reach the desired apolune position. Once the positional match is achieved, the second impulse, $\Delta\mathbf{v}_2 = \mathbf{v}_{apo} - \mathbf{v}_{target}$, is computed as the difference between the resulting velocity and the target velocity at apolune. In this way, both position and velocity matching are implicitly enforced through the root-finding procedure, even though no constraints are passed directly to the optimizer. Although this approach uses an unconstrained solver, the underlying formulation, seeking two $\Delta\mathbf{v}$ maneuvers that satisfy the full target state, remains unchanged.

6. Results

In this section, the boundaries used for the optimization variables and the results obtained are presented and discussed.

6.1 Transfer between two tori

Table 3 shows the optimization variables, the boundaries set and the results obtained for the optimization of the transfer between the tori. $t_{backprop}$ represents how in advance the first burn is performed with respect to the intersection point.

Table 3: Boundaries used for the optimization and results.

Variables	**Lower**	**Upper**	**Results**
$t_{backprop}$ [s]	1	10^5	216
$t_{coasting}$ [s]	1	10^5	571
Δv_1 [m/s]	6	36	21.8
Δv_2 [m/s]	1.8	36	14.5
σ_{1y} [deg]	0	360	35.9
σ_{1z} [deg]	0	360	201.9
σ_{2y} [deg]	0	360	44.9
σ_{2z} [deg]	0	360	217.5

The Δv vectors are computed through Equation 8 and are shown in Table 4.

This specific transfer is also simulated with a finite-burn maneuver, retrieving a total mass that differs from the one computed with the Tsiolkowsy equation for less than 0.01%, which proves that, in the case simulated, the assumption of impulsive maneuver is accurate. Given the result and being the focus of this paper on the methodology rather than on the accuracy of the propulsion model adopted, it has been decided not to further investigate finite-burn maneuvers in this work.

Table 4: Δv vectors in the rotating frame for the two-impulse transfer between the tori.

$\mathbf{\Delta v_1}$ [m/s]	$\mathbf{\Delta v_2}$ [m/s]
$[-16.4,\ -6.6,\ -12.8]$	$[-8.1,\ -6.2,\ -10.2]$

6.2 Rendezvous with the station

Table 5 shows the data used for the optimization and the results obtained.

Table 5: Boundaries used for the optimization and results.

Variables	**Lower**	**Upper**	**Results**
t_{prop} [s]	1	$5.6 \cdot 10^5$	$9.8864 \cdot 10^4$
$t_{coasting}$ [s]	1	$5.6 \cdot 10^5$	$2.3815 \cdot 10^5$
Δv_1 [m/s]	1	100	28.4
Δv_2 [m/s]	0.5	100	18.9
σ_{1y} [deg]	0	360	309.1
σ_{1z} [deg]	0	360	81.4
σ_{2y} [deg]	0	360	333.3
σ_{2z} [deg]	0	360	78.7

The Δv vectors are calculated and reported in Table 6.

Table 6: Δv vectors in the rotating frame.

$\mathbf{\Delta v_1}$ [m/s]	$\mathbf{\Delta v_2}$ [m/s]
$[2.7,\ 17.7,\ 22.0]$	$[3.3,\ 16.6,\ 8.5]$

6.3 Earth-NRHO transfer

Two simulations are performed, one aiming directly for the orbit of the Gateway, and another one aiming for the torus with ~ 120% period. Table 7 shows the results.

From the results, it can be noticed that, although the total transfer cost is increasing to get to the torus, the cost of the second maneuver is lower. However, the initial impulse will most likely be given by the launcher. This means that, considering only the maneuvers done by the spacecraft, there is an advantage in targeting the torus instead

Table 7: Optimization results.

Variables	Gateway	Torus
t_{prop} [s]	2403	2177
t_{coast} [days]	5.2254	5.4406
Δv_1 [m/s]	3179.8	3491.4
Δv_2 [m/s]	861.0	815.5

of the orbit of the Gateway for what regards this specific maneuver.

6.4 Wrap up

Once all the optimal transfers for the different legs are computed, it is possible to compare the results. In the first strategy the spacecraft is traveling directly to the station starting from LEO, in the second one, it is first traveling to the torus originated from the orbit with 120% the period of the Gateway, waiting parked there for a variable amount of time before moving to the torus around the target orbit, in the end the rendezvous is performed.

Table 8 sums up the results for the first strategy. The spacecraft has to deliver only 861 m/s out of the total because the rest is provided by the launcher to leave the Earth.

Table 8: Total Δv and traveling time, first strategy.

Operations	Δv [m/s]	Duration [days]
Reach escape point	–	0.0278
Escape Earth	3179.8	–
Reach the NRHO	–	5.225
NRHO insertion	861.0	–
Total	4040.8	5.253
Excluding launcher	861.0	5.225

In this case, the total number of maneuvers is low, but there is a direct correlation between the launch epoch and the arrival on the final orbit. This means that the launch epoch is constrained to the one needed to rendezvous correctly with the Gateway and, if that is not possible, an additional phasing maneuver becomes necessary, increasing the total propellant consumption.

Table 9 sums up the results for the strategy proposed in this work. The first value that stands out is the long transfer time. This is due to the wait time on the first torus before performing the maneuver, being about 577 days. This value is high due to the fact that, while designing the transfer, the minimum-Δv one is selected, regardless from the waiting time. However, looking back at Figure 17 it can be noticed that a large amount of low-cost transfers are available, also during the first few revolutions. In Table 10 are reported the transfer opportunities encountered during the first 10 revolutions and requiring less than $50\,m/s$ for the impulsive transfer. All the transfers shown in the table are close in terms of impulse required with the one previously selected and allow to reach the target, cutting down the transfer time. For example, using transfer number 1 (Table 10) the total transfer time becomes 31.3 days, a value much smaller than the previously retrieved one, and closer to the 5.3 days required by the direct strategy without accounting for the phasing.

Table 9: Total Δv and traveling time, strategy proposed in this work.

Operations	Δv [m/s]	Duration [days]
Reach escape point	–	0.0252
Escape Earth	3491.4	–
Reach torus	–	5.441
Torus insertion	815.5	–
Coasting on torus 1	–	576.898
Reach torus 2*	36.0	–
Coasting on torus 2	–	2.028
1^{st} rendezvous burn	20.9	–
Coasting	–	4.434
2^{nd} rendezvous burn	18.6	–
Total	4382.4	588.824
Excluding launcher	891.0	588.799
Change "*" with $N°1$ (Table 10)	892.0	~31.293

Table 10: Low-cost transfer opportunities during the first 10 revolutions.

Transfer $N°$	**Time** [days]	$\mathbf{\Delta v}$ [m/s]
1	19.3664	37.0
2	20.8983	38.5
3	26.6540	36.7
4	60.9250	49.1
5	66.6763	43.9

A more in depth study on the relative motion between the spacecraft on the initial torus and the Gateway on its orbit is performed. The goal is to prove that, after waiting on the first torus for the right amount of time, the spacecraft can rendezvous with the station requiring minimum or no phasing. If this is feasible regardless of the initial position of the Gateway at the arrival of the spacecraft on the torus, allows to decouple the launch date and the encounter epoch.

The analysis is performed considering only the transfers with an impulse lower than 50 m/s, and the initial position of the Gateway at the arrival of the spacecraft on the phasing torus (Torus 1) is computed as: $\theta_{1\ init} = \theta_{1\ transfer} - \omega_{1\ GW} t_{transfer}$. The choice of targeting the θ_1 of the Gateway is made to be compliant with the initial condition set in the trajectory optimization code to rendezvous with the station.

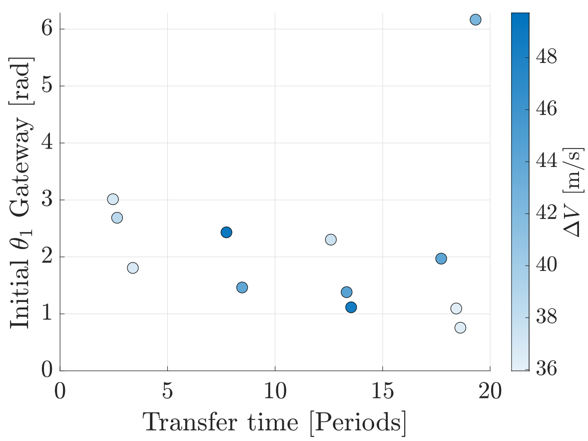

Fig. 21: Required initial θ_1 for the Gateway, zoom on the first 20 periods.

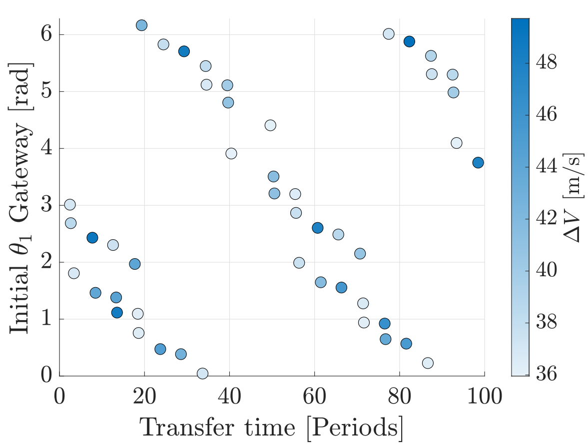

Fig. 22: Required initial θ_1 for the Gateway for the different transfer opportunities.

Figures 21 and 22 show that every transfer opportunity has a different initial phase of the station required (θ_1) to rendezvous correctly, covering a large variety of values. This shows that, in a large variety of cases, it is possible to complete the transfer with minimum or no phasing. If constraints on the mission duration are present, this method allows to enlarge the launch window by providing different transfer options respecting the constraints. It is however evident that the flexibility grows significantly while looser constraint on the total transfer duration are imposed.

6.4.1 Strategy to shorten mission duration

The first that can be noticed is that in general the method offers larger flexibility in mission design for a relatively small increase of impulse required for the mission (about 4%). What stands out, however is the large increase in transfer time, even if the first low-cost transfer opportunity available is used, being almost 600%. It was therefore decided to investigate a strategy to overcome this problem: the idea is to target a different branch of the first torus while performing the transfer from LEO, choosing a value of θ_2 that is conveniently providing a transfer opportunity in a matter of few days for a known initial position of the Gateway at the arrival on torus 1. In this case, the analysis has been carried out at regular intervals of 30 degrees on the value of θ_2, retrieving the first transfer opportunity below 50 m/s and the required initial position for the station to rendezvous correctly. Table 11 shows the results of this analysis, from the data retrieved is possible to notice that is possible to cut down the transfer time by up to an additional 16 days depending on the initial position of the station.

Table 11: Transfer opportunities for different initial θ_2 of insertion on torus 1.

$\boldsymbol{\theta}_{\mathbf{2i}}$ [deg]	$\boldsymbol{\theta}_{\mathbf{1i}}$ GW [deg]	$\mathbf{t_{wait}}$ [days]	$\mathbf{\Delta v}$ [m/s]
0	172.6	19.3664	37.0
30	232.6	12.4876	38.8
60	243.9	11.7246	42.7
90	304.4	4.8606	36.0
120	301.2	5.7023	46.7
150	326.0	3.0794	37.9
180	318.8	3.7544	48.6
210	329.0	2.6663	40.6
240	78.8	28.7412	36.7
270	21.3	35.2169	46.1
300	150.9	21.3899	42.9
330	160.9	20.1928	46.4

The transfer with minimum transfer time required has been fully simulated to make sure that also the other transfers are feasible and retrieve the new total mission cost and time. Table 12 shows the results for the strategy exploiting the tori with the new approach to shorten the transfer time, it can be noticed a significative decrease of transfer time at the price of a small increase in required impulse. If required, the rendezvous maneuver could be performed at the arrival on the second torus, without any waiting time on it. This will add a few m/s of impulse required, but will save some days of transfer time.

Table 12: Total Δv and traveling time, strategy aiming to cut down the total transfer time.

Operations	Δv **[m/s]**	**Duration [days]**
Reach escape point	–	0.0248
Escape Earth	3505.2	–
Reach torus	–	5.338
Torus insertion	835.0	–
Coasting on torus 1	–	2.666
Reach torus 2	40.6	–
Coasting on torus 2	–	5.333
1^{st} rendezvous burn	19.7	–
Coasting	–	4.197
2^{nd} rendezvous burn	18.6	–
Total	4419.1	17.559
Excluding launcher	913.9	17.534

In conclusion, depending on the available launch epochs, position of the Gateway in those epochs and mission constraints given by the nature of the mission itself, the direct strategy can be compared with the one proposed in this paper, keeping in mind advantages and disadvantages of both for the specific mission under design. It is likely that in manned missions, in which time is critical, the propellant savings are not a driver, and the launch date can be adjusted more freely, having as a priority the safety of the astronauts and the sustainability of the travel for the humans onboard. On the other side, for cargo missions, depending on the payload, the priority could be to have more flexibility in the choice of the launch epoch rather than reaching the station faster.

7. Conclusions

In this paper it is shown that the interpolation method adopted works properly to retrieve analytical curves from which intersection points and transfer opportunities are extracted. The results show that the accuracy is in the order of km for the distances and m/s for the velocities, assessing the suitability of those curves to retrieve good initial guesses to design a transfer. This concept has been further developed, proving that the interpolation method is capable of ensuring the required accuracy, also in the case of tori with a less regular shape, the only tuning needed is to adjust the number of nodes (n_{nodes}).

In the end, the mission from a LEO to the Gateway is simulated, comparing the results obtained with the method presented in this work with a strategy traveling directly to the station. In light of the results presented, two key trade-offs emerge. The direct LEO to Gateway transfer requires a total Δv of approximately 861 m/s post-escape, and completes in only ~ 5.3 days, but rigidly fixes the launch epoch to the Gateway's phase, often forcing additional phasing maneuvers. On the other hand, the torus-assisted strategy requires a slightly higher post-escape Δv (913.9 m/s), yet decouples launch timing: by choosing the desired low-cost impulsive hop on the 120%-period torus, it is possible retrieve transfer times in the order of few weeks, while offering a wide range of rendezvous epochs and minimizing or even eliminating final phasing maneuvers. Hence, depending on whether mission objectives prioritize minimum transfer time or maximum propellant efficiency and flexible launch windows, each approach provides a distinct balance of Δv budget, duration, and operational freedom.

8. Further developments

During the development of this work, several ideas for future research that can further refine and extend the capabilities of this methodology are individuated:

- **Investigate Different Interpolation Methods.** While cubic spline interpolation has proven effective for representing tori, Fourier has not nearly achieved the desired accuracy. However, the advantage of having a unique interpolating function valid in the entire domain instead of a piecewise one will allow more flexibility and numerical efficiency during the continuation process to retrieve the interpolating curves. At the same time, being the cubic spline C^2 at the intersection points there are no problems related to discontinuities. Moreover, alternative approaches, such as radial basis functions, Chebyshev polynomials, or wavelet-based interpolants, may offer improved local accuracy, especially in regions where the torus geometry exhibits rapid curvature changes.
- **Target the Torus rather than a Specific Orbit.** The current transfer targets a specific trajectory branch on torus 2. By relaxing this constraint and instead targeting the torus manifold as a whole, it can be possible to exploit a continuum of arrival conditions. This flexibility can reduce Δv costs and increase the flexibility on the transfer, enhancing launch window opportunities. On top of that targeting a specific branch of the torus allowing to complete the transfer sooner would

cut down the total transfer time.

- **Global Optimization of Coupled Transfer Segments.** The present approach optimizes each leg of the transfer sequentially. A natural extension is to formulate a single, coupled optimization problem that simultaneously adjusts all departure, coast, and insertion phases. Such a global optimization scheme would better capture trade-offs between waiting time on the initial torus and insertion accuracy at the final torus, yielding truly minimal-cost solutions. Although the development of this algorithm is straightforward once every leg has been simulated, the need of a powerful computing machine becomes necessary due to the large number of optimization variables and constraints to satisfy.
- **Seamless Torus-to-Torus Transitions and Manifold Exploitation.** Future work can explore the design of trajectories that smoothly hop between a sequence of invariant tori, gradually advancing toward the target region. By leveraging adjacent torus intersections and ultimately exploiting the stable manifold of the final torus, the terminal rendezvous can be achieved with minimal Δv, taking advantage of natural dynamical highways for cost-effective station access.
- **Adopt Higher-Accuracy Dynamical Models and Ephemerides.** To bridge the gap between CR3BP approximations and mission-level precision requirements, the framework should be extended to more realistic dynamical environments. Incorporating ephemeris-based models, solar perturbations, non-spherical gravity terms, and solar radiation pressure will enhance the fidelity of trajectory predictions and support the design of operational transfer strategies. These models will also allow to exploit the state of the art transfer to the Gateway developed by NASA [14, 15], allowing also a more accurate comparison between the two rendezvous strategies.
- **Investigate Low-Thrust Transfer Strategies.** The integration of continuous low-thrust propulsion (such as electric propulsion) into the torus intersection framework can further reduce propellant consumption to move from the initial torus to the station. By coupling thrust-level, duration, and trajectory shaping in a unified optimization, extended low-energy pathways can be exploited while accommodating mission constraints such as power availability and thrust arcs. This strategy is already under development within the research group.

By pursuing these developments, the torus-intersection methodology will mature into a more robust and versatile tool for low-energy mission design, capable of addressing both theoretical challenges and practical mission constraints.

References

[1] US Code. United states code. *Subtitle F*, 2018.

[2] James A Vedda. Cislunar development: What to build and why. *The Aerospace Corporation*, 2018.

[3] Marcus J Holzinger, C Channing Chow, and Peter Garretson. *A primer on cislunar space*. Air Force Research Laboratory Greene County, OH, USA, 2021.

[4] Damennick B Henry and Daniel J Scheeres. Quasi-periodic orbit transfer design via whisker intersection sets. *Journal of Guidance, Control, and Dynamics*, 46(10):1929–1944, 2023.

[5] Dhruv Jain and Kathleen Howell. Leveraging quasi-periodic orbits to design transfers in the circular restricted three-body problem. In *AIAA SCITECH 2024 Forum*, page 0841, 2024.

[6] Marcel Duering. *Station-keeping and orbital transfers in the vicinity of the Moon exploiting quasi-periodic orbit dynamics*. PhD thesis, University of Strathclyde, 2020.

[7] Brian P McCarthy and Kathleen C Howell. Leveraging quasi-periodic orbits for trajectory design in cislunar space. *Astrodynamics*, 5(2):139–165, 2021.

[8] Dhruv Jain. Transfer trajectory design strategies informed by quasi-periodic orbits. Master's thesis, Purdue University, 2023.

[9] Fabio Ferrari. Formation flying dynamics in circular restricted three body problem and applications to binary asteroid systems. Master's thesis, Politecnico di Milano, 2012.

[10] Nicola Baresi, Zubin P Olikara, and Daniel J Scheeres. Fully numerical methods for continuing families of quasi-periodic invariant tori in astrodynamics. *The Journal of the astronautical sciences*, 65:157–182, 2018.

[11] Emily M Zimovan Spreen. *Trajectory design and targeting for applications to the exploration program in cislunar space*. PhD thesis, Purdue University, 2021.

[12] Zubin P Olikara and Daniel J Scheeres. Numerical method for computing quasi-periodic orbits and

their stability in the restricted three-body problem. *Advances in the Astronautical Sciences*, 145(911-930):911–930, 2012.

[13] Emily M Zimovan. Characteristics and design strategies for near rectilinear halo orbits within the earth-moon system. Master's thesis, Purdue University, 2017.

[14] Ryan J Whitley, Diane C Davis, Laura M Burke, Brian P McCarthy, Rolfe J Power, Melissa L McGuire, and Kathleen C Howell. Earth-moon near rectilinear halo and butterfly orbits for lunar surface exploration. In *AAS/AIAA Astrodynamics Specialists Conference, Snowbird, Utah*, 2018.

[15] Diane C. Davis, Emily M. Zimovan-Spreen, Stephen T. Scheuerle, and Kathleen C. Howell. Dynamics of jettison during earth-to-nrho transfers. *Acta Astronautica*, 2025.